Journal of Luminescence 130 (2010) 206–210

Contents lists available at ScienceDirect

Journal of Luminescence

journal homepage: www.elsevier.com/locate/jlumin

Review

Red photoluminescence due to energy transfer from Eu^{2+} to Cr^{3+} in $BaAl_{12}O_{19}$

Ruixia Zhong, Jiahua Zhang *

Key Laboratory of Excited State Processes, Changchun Institute of Optics, Fine Mechanics and Physics, Chinese Academy of Sciences, 16 Eastern South Lake Road, Changchun 130033, China

ARTICLE INFO

Article history:
Received 30 September 2008
Received in revised form
9 September 2009
Accepted 18 September 2009
Available online 30 September 2009

Keywords:
Energy transfer
Cr^{3+}
Eu^{2+}
Red photoluminescence
$BaAl_{12}O_{19}$

ABSTRACT

$BaAl_{12}O_{19}$–$BaAl_2O_4$ doped with Eu^{2+}, Cr^{3+} and (Eu^{2+}+Cr^{3+}) are prepared by solid-state reaction. The spectra of $BaAl_{12}O_{19}$–$BaAl_2O_4$:Eu^{2+}, Cr^{3+} shows that the f–d emission bands from Eu^{2+} are centered at 442 and 495 nm and the Cr^{3+} yields the emission lines at 694 and 700 nm. Photoluminescence study demonstrates that the red photoluminescence and energy transfer occurs only in the phase of $BaAl_{12}O_{19}$ not $BaAl_2O_4$ though the samples are mixed phases. The fluorescence lifetime measurements indicate efficient energy transfer from Eu^{2+} to Cr^{3+} in $BaAl_{12}O_{19}$: Eu^{2+}, Cr^{3+}. The energy transfer rate and efficiency are calculated. The results show that the energy transfer rate and efficiency increase following the increase in Cr^{3+} concentration.

Contents

1. Introduction

Much attention has been paid to the development of advanced luminescent materials for applications such as flat panel displays, Hg-free lamps and X-ray imaging systems. Among the various types of flat panel displays are plasma display panels, which have a competitive edge in the large-screen display market [1–3]. In the initial devices, the conventional phosphors such as Y_2O_3:Eu and (Y, Gd)BO_3:Eu for red, $BaMgAl_{10}O_{17}$:Eu for blue and Zn_2SiO_4:Mn for green, which were already established as lamp/CTV phosphors, were used as PDP materials. However, several problems arise. For example, the cost of Y_2O_3:Eu phosphor is too much [4]. Zn_2SiO_4:Mn is known to have a long decay time and a high discharging voltage [5]. $BaMgAl_{10}O_{17}$:Eu degrades fast. In order to improve the performance of PDP devices, novel phosphors with high luminescent efficiency and stability have been searched.

$BaAl_{12}O_{19}$, as a host, has attracted much attention for its good stability adaptable for displays and lamps such as plasma display panels (PDPs) [6], field emission displays (FEDs) and Hg-free lamps, such as $BaAl_{12}O_{19}$:Mn^{2+} [7] and $BaAl_{12}O_{19}$:Eu^{2+} [8]. Although so many phosphors using $BaAl_{12}O_{19}$ as hosts have been developed, there is no red phosphor among them.

As we know, the Cr^{3+} ion with red emission is one of the most used activators for solid-state laser [9,10] and luminescent materials [11]. At the same time, the Cr ions as activators have low cost. Presently, we have reported the efficient energy transfer from Eu^{2+} to Cr^{3+} in $Sr_4Al_{14}O_{25}$ [12,13], $SrAl_{12}O_{19}$ [14] and $Sr_3Al_{10}SiO_{20}$ [15]. Hence, our experiments are extended to study the energy transfer processes in Eu^{2+}, Cr^{3+} co-doped $BaAl_{12}O_{19}$.

In this paper, we report the photoluminescence characteristics of $BaAl_{12}O_{19}$–$BaAl_2O_4$:Eu^{2+}, Cr^{3+}. The energy transfer from Eu^{2+} to Cr^{3+} and the red emission of Cr^{3+} have only been observed in the phase of $BaAl_{12}O_{19}$. The energy transfer rate and efficiency in the phase of $BaAl_{12}O_{19}$ are calculated and discussed.

2. Experiments

Samples of $BaAl_{12}O_{19}$–$BaAl_2O_4$:Eu^{2+}, Cr^{3+} have been synthesized by high-temperature solid-state reaction. The starting materials are $BaCO_3$ (AR), Al_2O_3 (AR), Eu_2O_3 (99.9%), Cr_2O_3 (AR)

* Corresponding author. Tel./fax: +86 335 805 6635.
E-mail address: zhongruixialiu@yahoo.com.cn (R. Zhong).

0022-2313/$ - see front matter © 2009 Elsevier B.V. All rights reserved.
doi:10.1016/j.jlumin.2009.09.021

and H_3BO_3 (AR). The powder samples have been weighed according to the molar ratio given by the formula. All the mixtures are ground for 1 h, then sintered at 1550 °C in a reducing atmosphere for 4 h. For comparison, the sample $BaAl_2O_4$:Eu^{2+}, Cr^{3+} has also been prepared by high-temperature solid-state reaction at 1500 °C.

Emission and excitation spectra are measured with a Hitachi F-4500 Spectra-fluorometer. In fluorescence lifetime measurements, the fourth (266 nm) harmonic of a Nd-YAG laser (Spectra-Physics, GCR 130) is used as an excitation source, and the signal is detected with a Tektronix digital oscilloscope model (TDS 3052). The crystalline structure of the sample is investigated by X-ray diffraction (XRD), using a Siemens D-500 equipment with a Cu target radiation source.

3. Results and discussion

XRD patterns of our sample $BaAl_{12}O_{19}$–$BaAl_2O_4$:Eu^{2+}, Cr^{3+}, $BaAl_2O_4$:Eu^{2+}, Cr^{3+}, the standard $BaAl_{12}O_{19}$ pattern (JCPDS-no. 26–0135) and standard $BaAl_2O_4$ pattern (JCPDS-no. 17–0306) are shown in Fig. 1. The X-ray diffraction peaks of our sample $BaAl_{12}O_{19}$–$BaAl_2O_4$:Eu^{2+}, Cr^{3+} match well with the standard $BaAl_{12}O_{19}$ pattern (JCPDS-no. 26–0135) except the peak at 28°. The peak at 40° belongs to the $BaAl_{12}O_{19}$ pattern as well as to the $BaAl_2O_4$ pattern. The pure $BaAl_{12}O_{19}$ can be indexed on the space group $P6_3/mmc$ for hexagonal $BaAl_{12}O_{19}$ with the magnetoplumbite-type structure. The XRD pattern of the synthesized sample $BaAl_2O_4$ has matched with JCPDS (17–0306). The pure $BaAl_2O_4$ belongs to the space group $P6_322$.

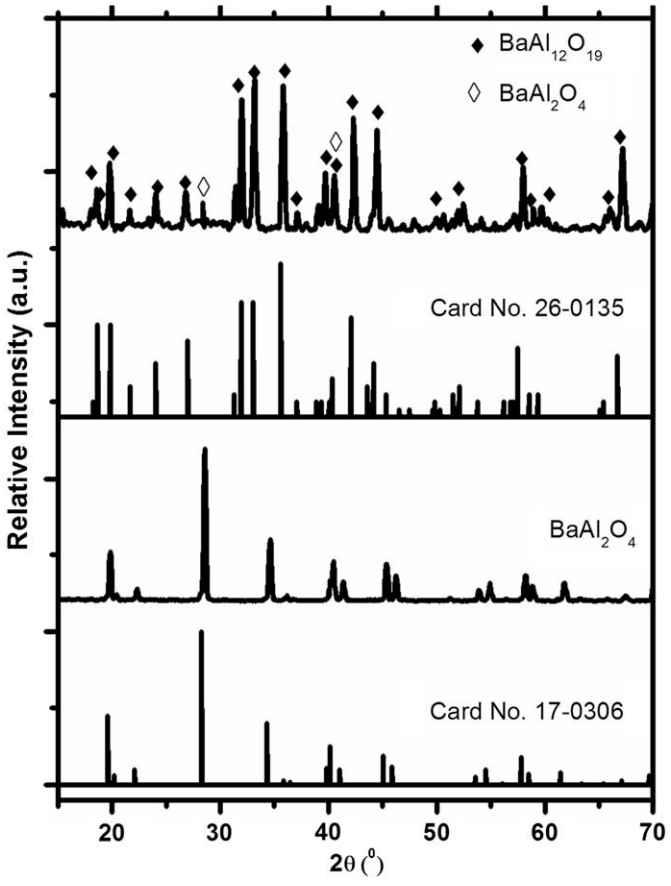

Fig. 1. XRD patterns of our sample $BaAl_{12}O_{19}$–$BaAl_2O_4$:Eu^{2+}, Cr^{3+}, $BaAl_2O_4$:Eu^{2+}, Cr^{3+}, the standard $BaAl_{12}O_{19}$ pattern (JCPDS-no. 26–0135) and standard $BaAl_2O_4$ pattern (JCPDS-no. 17–0306).

Fig. 2 shows the excitation and emission spectra of $BaAl_2O_4$:1% Eu^{2+}, 1% Cr^{3+} [Fig. 2(a)] and $BaAl_{12}O_{19}$–$BaAl_2O_4$:1% Eu^{2+}, 1% Cr^{3+} [Figs. 2(b) and (c)]. Both the emission and excitation spectra of $BaAl_2O_4$:1% Eu^{2+}, 1% Cr^{3+} [Fig. 2(a)] are broad bands, which can be assigned to 5d–4f transition of Eu^{2+}. The emission band from Eu peaks at 495 nm and excitation band peaks at 306 nm. Although the Cr^{3+} ions as activators are incorporated into $BaAl_2O_4$ host, the red or infrared luminescence from Cr^{3+} ions is not observed. There only exists AlO_4 tetrahedra in the $BaAl_2O_4$ host. The Cr^{3+} ions are incorporated into the host to replace the Al ions in the AlO_4 tetrahedra. As we know, the electrons on the ^2E or $^4T_2$ level return

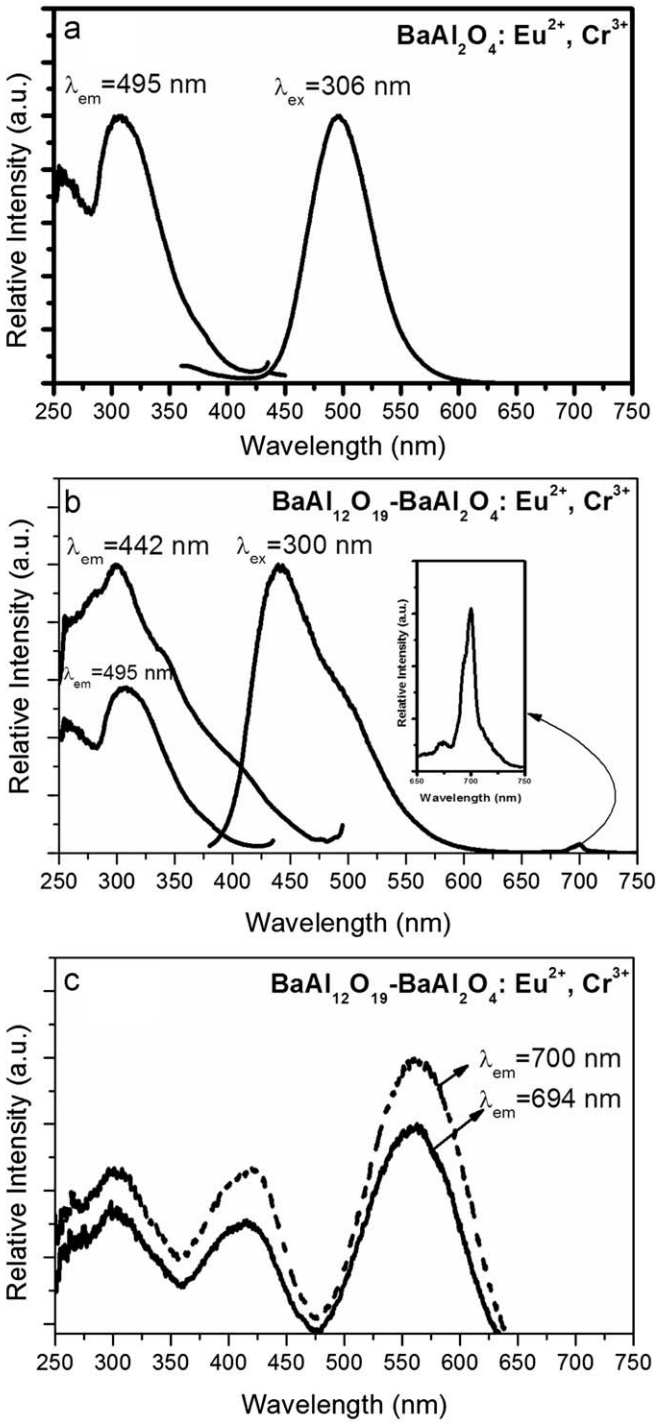

Fig. 2. Excitation and emission spectra of $BaAl_2O_4$:1% Eu^{2+}, 1% Cr^{3+} [Fig. 2(a)] and $BaAl_{12}O_{19}$–$BaAl_2O_4$:1% Eu^{2+}, 1% Cr^{3+} [Figs. 2(b) and (c)].

to the $^4A_2$ level in octahedral crystal field and yield the red or infrared light [16]. There is no AlO_6 octahedron in the $BaAl_2O_4$ host, so the Cr^{3+} ions give no emission light in $BaAl_2O_4$:1% Eu^{2+}, 1% Cr^{3+}. In Fig. 2(b), the emission spectra consist of two emission bands and two emission lines. The two broad bands are originating from Eu ions: the main peak centers at 442 nm and the shoulder peak centers at 495 nm. The spectrum inside is enlarged Cr^{3+} emission spectrum. From the enlarged Cr^{3+} emission spectrum, two emission lines are observed: the main line peaks at 700 nm and the shoulder line peaks at 694 nm. Both of the emission lines are originating from ^2E–$^4A_2$ transitions. Comparing the excitation and emission spectra in Fig. 2(b) with those in Fig. 2(a), it is worth noting that the emission and excitation spectra for 495 nm emission center in the mixed phase of $BaAl_{12}O_{19}$–$BaAl_2O_4$:1% Eu^{2+}, 1% Cr^{3+} are same as those in the phase of $BaAl_2O_4$:1% Eu^{2+}, 1% Cr^{3+}. It indicates that the emission band centered at 442 nm is from f–d transition of Eu in the phase of $BaAl_{12}O_{19}$: 1% Eu^{2+}, 1% Cr^{3+}. The two emission lines for Cr are also from ^2E–$^4A_2$ transitions in the phase of $BaAl_{12}O_{19}$: 1% Eu^{2+}, 1% Cr^{3+} because of no Cr emission line appears in the phase of $BaAl_2O_4$:1% Eu^{2+}, 1% Cr^{3+}. The excitation spectra of 694 and 700 nm emission lines are shown in Fig. 2(c). The two excitation spectra are almost the same but the emission spectra are different. It means that there exist two different emission centers for Cr ions in the phase of $BaAl_{12}O_{19}$: 1% Eu^{2+}, 1% Cr^{3+}. Due to the small difference in emission spectra and broad excitation bands, the excitation spectra of the two emission centers are the same.

Fig. 3 depicts the emission and excitation spectra of $BaAl_{12}O_{19}$–$BaAl_2O_4$:x% Eu^{2+}, 1% Cr^{3+} (x=0, 0.5, 1, 2 and 3): (a) λ_{em}=694 nm; (b) λ_{em}=700 nm. In $BaAl_{12}O_{19}$–$BaAl_2O_4$:x% Eu^{2+}, 1% Cr^{3+} (x=0.5, 1, 2 and 3), both the ^2E–$^4A_2$ emissions of Cr^{3+} at 694 and 700 nm are observed under 306 nm excitation. The excitation spectra of the 694 [Fig. 3(a)] and 700 nm emissions [Fig. 3(b)] are the same and they consist of the $^4A_2$–$^4T_1$ (F) absorption at 400 nm and $^4A_2$–$^4T_2$ (F) absorption at 565 nm of Cr^{3+}, and the f–d absorption of Eu^{2+} in ultraviolet region. The intensities of the 565 nm excitation bands are normalized. From Figs. 2(b) and 3, the 442 nm emission band of Eu^{2+} has spectral overlaps with the absorption bands of Cr^{3+}, indicating the possibility of energy transfer from Eu^{2+} to Cr^{3+}. It can also be seen that the excitation bands originating from f–d transition of Eu^{2+} in ultraviolet region grow up with increase in Eu^{2+} concentrations when the red emission at 694 and 700 nm of Cr^{3+} are monitored until the Eu^{2+} concentration is up to 3%. Furthermore, the red emission of Cr^{3+} increases with increase in Eu^{2+} concentrations under 306 nm excitation, by which only Eu^{2+} can be excited because there is no absorption of Cr^{3+} at this wavelength as shown in Fig. 3. These results strongly indicate the performance of energy transfer from Eu^{2+} to the Cr^{3+} ions with different environments in $BaAl_{12}O_{19}$: Eu^{2+}, Cr^{3+}.

Fig. 4 shows the emission spectra of $BaAl_{12}O_{19}$–$BaAl_2O_4$:1% Eu^{2+}, x% Cr^{3+} (x=0.5, 1, 2, 3, 4 and 5) under 306 nm excitation, where the intensities of the blue bands at 442 nm are normalized. When maintaining the Eu^{2+} concentration and increasing the Cr^{3+} contents up to 5%, the red lines at 694 and 700 nm from Cr^{3+} are enhanced, indicating increase in energy transfer efficiency since Cr^{3+} cannot be excited by 306 nm directly. The addition of Cr^{3+} ions leads to an increase in Cr^{3+} surrounding the Eu^{2+} ion, thus resulting in more efficient energy transfer. As we know, the concentration of Cr^{3+} does not affect the change of phases in this system. Thus, the ratio of the number of Eu in the phase of $BaAl_{12}O_{19}$ to the number of Eu in the phase of $BaAl_2O_4$ can be considered as constant. From the emission spectra in Fig. 4, the emission band from Eu in $BaAl_2O_4$ phase increases relatively to

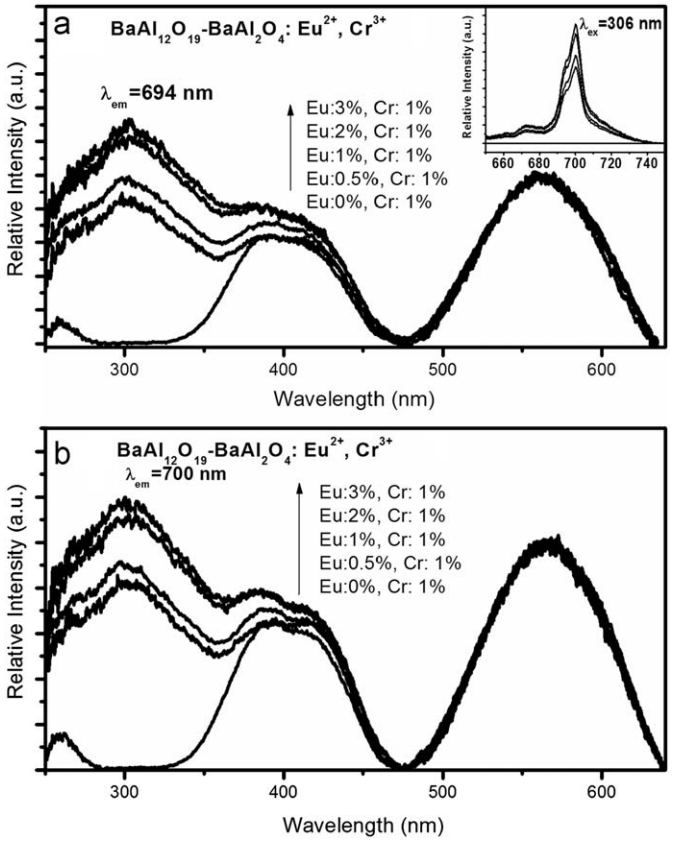

Fig. 3. Excitation spectra of $BaAl_{12}O_{19}$–$BaAl_2O_4$:x% Eu^{2+}, 1% Cr^{3+} (x=0, 0.5, 1, 2 and 3): (a) λ_{em}=694 nm and (b) λ_{em}=700 nm. Inset of Fig. 3a is emission spectra of $BaAl_{12}O_{19}$–$BaAl_2O_4$:x% Eu^{2+}, 1% Cr^{3+} (x=0, 0.5, 1, 2 and 3, λ_{ex}=306 nm).

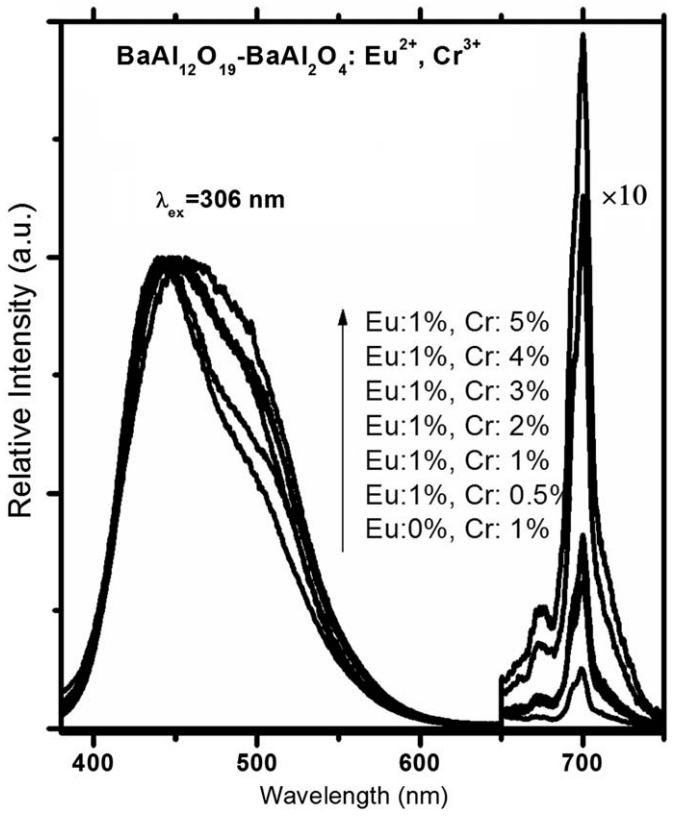

Fig. 4. Emission spectra of $BaAl_{12}O_{19}$–$BaAl_2O_4$:1% Eu^{2+}, x% Cr^{3+} (x=0.5, 1, 2, 3, 4 and 5) under 306 nm excitation, where the intensities of the blue bands at 442 nm are normalized.

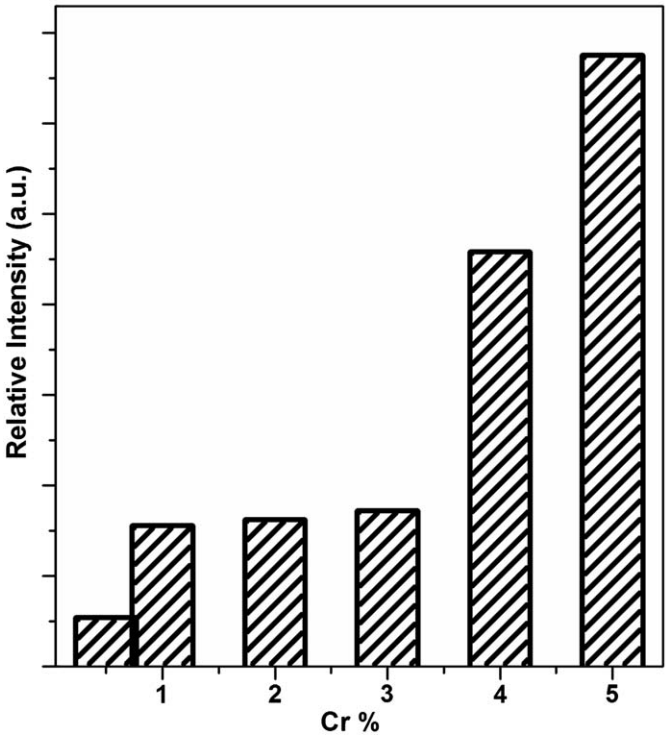

Fig. 5. Dependence of the ratio for the red emission to the blue one on the Cr^{3+} concentration.

those in $BaAl_{12}O_{19}$ phase. It is because the energy transfer from Eu to Cr happens in the phase of $BaAl_{12}O_{19}$. According to the emission spectra shown in Fig. 4, the intensity ratios of the red emission of Cr^{3+} to the blue emission of Eu^{2+} are plotted as a function of Cr^{3+} concentrations, as shown in Fig. 5. The ratio grows up with increase in Cr^{3+} concentration. It means that the blue emission can be partly converted to the red one and the ratio of the red to the blue can be controllable by changing the concentration of Eu and Cr.

In order to analyze the energy transfer rate and efficiency as a function of Cr^{3+} concentration, the fluorescence decay curves of 442 nm emissions originating from Eu^{2+} in the phase of $BaAl_{12}O_{19}$ doped with 1% Eu^{2+}, x% Cr^{3+} (x=0.5, 1, 2, 3, 4 and 5) are measured and presented in Fig. 6. As we know, if the average donor–acceptor transfer rate is larger than the donor–donor diffusion rate, the donors will depart from single exponential decay [17,18]. Thus, the decay patterns shown in Fig. 6 slightly depart from single exponential function at the high concentration of Cr^{3+}. According to Inokuti–Hirayama model, the lifetime can be obtained by the following definition [19]:

$$\tau = \frac{1}{I_0}\int_0^{\infty} I(t)\,dt \tag{1}$$

where I_0 is the fluorescence intensity at the time t=0. According to the Eq. (1), the lifetimes of Eu^{2+} in the phase of $BaAl_{12}O_{19}$ at different Cr concentrations are shown in Fig. 6 (inset). The lifetimes of Eu^{2+} (τ_{blue}) reduce with increase in Cr^{3+} concentration because of the energy transfer from Eu^{2+} to Cr^{3+}. As is known, the macroscopic energy transfer rate W_{Eu-Cr} as a function of Cr^{3+} concentration can be evaluated from the lifetime measurement since

$$W_{Eu\text{-}Cr} = 1/\tau_{blue} - 1/\tau_{blue,0} \tag{2}$$

where $\tau_{blue,0}$ is the intrinsic decay lifetime of Eu^{2+}. When the concentration of Cr^{3+} is low, the energy transfer rate is too small to be ignored. Thus, the lifetime of Eu^{2+} in $BaAl_{12}O_{19}$–$BaAl_2O_4$:1% Eu^{2+}, 0% Cr^{3+} can be recognized as the intrinsic decay lifetime.

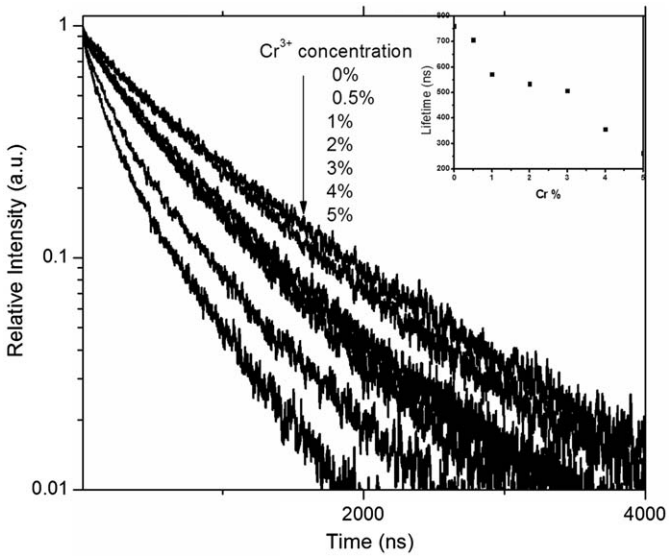

Fig. 6. The fluorescence decay curves of 442 nm (τ_{blue}) emissions for different Cr^{3+} concentrations; the lifetimes of 442 nm (τ_{blue}) emissions versus Cr^{3+} concentrations are presented in the inset.

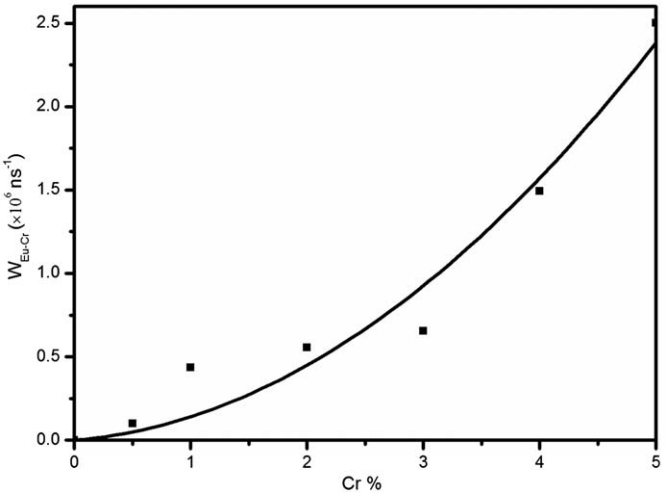

Fig. 7. Dependence of the energy transfer rate on the Cr^{3+} concentration.

According to Eq. (2), the energy transfer rate has been obtained and shown in Fig. 7. The energy transfer rate between Eu and Cr is considered to be the relationship with the Cr concentration, which can be described as a function of $W_{Eu\text{-}Cr} = aC_{Cr}^2 + bC_{Cr}$, where C_{Cr} is the Cr^{3+} concentration; a and b are the constants for the energy transfer rate. The calculated curves are also drafted in Fig. 7. The values of a and b are, respectively, $8.39\times10^4\,s^{-1}\,mol^{-2}$ and $5.73\times10^4\,s^{-1}\,mol^{-1}$. The calculated curve perfectly agrees with the experimental data. The energy transfer rate increases following the Cr^{3+} concentration. The enhancement of the number of Cr ions surrounding the Eu ions leads to short distance between Eu and Cr, so the energy transfer rate becomes fast.

The energy transfer efficiency (η_T) as a function of Cr^{3+} is also investigated. According to the definition suggested by Paulous [20], η_T can be expressed by

$$\eta_T = 1 - \frac{\tau_{blue}}{\tau_{blue,0}} \tag{3}$$

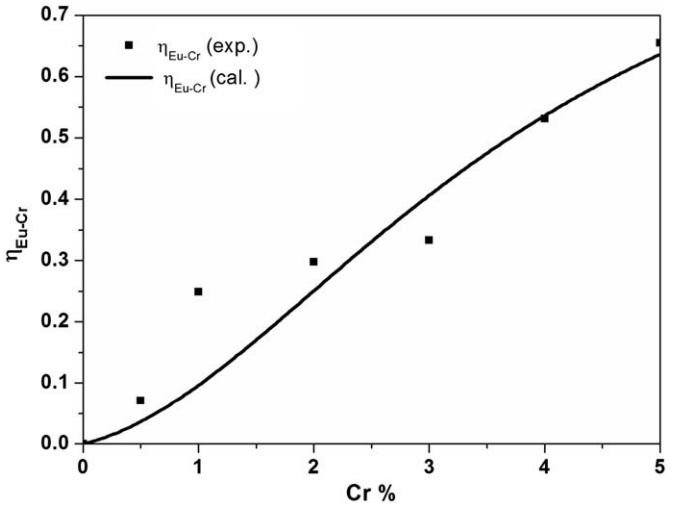

Fig. 8. Dependence of the energy transfer efficiency on the Cr^{3+} concentration

Using Eq. (3) and the measured lifetimes, the energy transfer efficiency has been obtained and shown in Fig. 8. The calculated curves in Fig. 8 are drafted according to the relationship between the energy transfer rate (W_{Eu-Cr}) and energy transfer efficiency (η_T) expressed by

$$\eta_T = 1 - \frac{1}{\tau_{blue,0}(aC_{Cr}^2 + bC_{Cr}) + 1} \quad (4)$$

The calculated curves show reasonable agreement with the experimental data. With increase in Cr^{3+} concentration, the transfer efficiency in $BaAl_{12}O_{19}$ phase increases.

As the discussion above, the Cr ions with different environments in the phase of $BaAl_{12}O_{19}$ give two sharp emission lines from ^2E–$^4A_2$ transitions. The high efficient energy transfer from Eu to the different Cr occurs in the co-doped samples. Due to the efficient energy transfer and stable matrix, the phosphor $BaAl_{12}O_{19}$:Eu, Cr will be a promising red luminescent material with high luminescence efficiency, good stability and low cost.

4. Conclusions

In summary, the energy transfer has been observed in the phase of $BaAl_{12}O_{19}$ with Eu, Cr co-doped, which leads to the following results: (1) the intensity of the red emission of Cr^{3+} is enhanced by increase in the concentration of optically excited Eu^{2+}; (2) as the concentration of Eu^{2+} is fixed, the ratio of the red emission to the blue of Eu^{2+} increases with increase in Cr^{3+} concentration when only Eu^{2+} is optically excited. The energy transfer rate and efficiency increases following Cr^{3+} concentration. Therefore, the red emission can be obtained by converting the blue emission from Eu^{2+}. Because of its good stability and efficient energy transfer, the phosphor $BaAl_{12}O_{19}$: Eu^{2+}, Cr^{3+} will be a promising red luminescent material for illumination and display.

References

[1] T. Justel, H. Nikol, C. Ronda, Angew. Chem. Int. Ed. 37 (1998) 3084.
[2] G. Blasse, B.C. Grabmaier, Luminscent Materials, Springer-Verlag, Berlin, 1994.
[3] J. Wang, Y. Yoo, C. Gao, I. Takeuchi, X. Sun, H. Chang, X.D. Xiang, G. Schults, Science 279 (1998) 1712.
[4] C.K. Lin, M.L. Pang, M. Yu, J. Lin, J. Lumin. 114 (2005) 299.
[5] S.W. Lu, T. Copeland, B.I. Lee, W. Tong, B.K. Wagner, W. Park, F. Zhang, J. Phys. Chem. Solids 62 (2001) 777.
[6] K.S. Sohn, E.S. Park, C.H. Kim, H.D. Park, J. Electrochem. Soc. 147 (2000) 4368.
[7] Y.H. Wang, F. Li, J. Lumin. 122–123 (2007) 866.
[8] H.S. Jeon, S.K. Kim, H.L. Park, G.C. Kim, J.H. Bang, M. Lee, Solid State Commun. 120 (2001) 221.
[9] Y. Qui, J. Phys.: Condens. Matter 5 (1993) 2041.
[10] A.A. Kaminskii, Crystalline Lasers: Physical Processes and Operating Schemes, CRC Press, Boca Raton, 1996.
[11] J.E. Geusic, H.M. Marcos, L.G. Van Uitert, Appl. Phys. Lett. 4 (1964) 182.
[12] R.X. Zhong, J.H. Zhang, X. Zhang, S.Z. Lu, X.J. Wang, J. Lumin. 119–120 (2006) 327.
[13] R.X. Zhong, J.H. Zhang, X. Zhang, S.Z. Lu, X.J. Wang, Appl. Phys. Lett. 88 (2006) 201916.
[14] R.X. Zhong, J.H. Zhang, X. Zhang, S.Z. Lu, X.J. Wang, Nanotechnology 18 (2007) 445707.
[15] R.X. Zhong, J.H. Zhang, X. Zhang, S.Z. Lu, X.J. Wang, J. Phys. D: Appl. Phys. 41 (2008) 065104.
[16] S.A. Basun, A.A. Kaplyanskii, A.B. Kutsenko, V. Dierolf, V. Troester, S.E. Kapphan, K. Polgar, Appl. Phys. B 73 (2001) 453.
[17] M.M. Broer, D.L. Huver, W.M. Yen, W.K. Zwicker, Phys. Rev. Lett. 49 (1982) 394.
[18] M.M. Broer, D.L. Huver, W.M. Yen, W.K. Zwicker, Phys. Rev. B 29 (1984) 2382.
[19] Mitto Inokuti, Fumio Hirayama, J. Chem. Phys. 43 (1965) 1978.
[20] P.I. Paulose, G. Jose, V. Thomas, N.V. Unnikrishnan, M.K.R. Warrier, J. Phys. Chem. Solids 64 (2003) 841.